



The Effect of Gd Additions on the Oxidation Resistance of TiAl Alloys Prepared by SPS

Qianqian Guo¹ · Hongliang Sun¹ · Zhengkun Cai¹ · Yuxing Deng¹ · Xiaosong Jiang¹ · Song Chen¹

Received: 9 July 2021 / Revised: 30 November 2021 / Accepted: 2 December 2021 /
Published online: 19 January 2022

© The Author(s), under exclusive licence to Springer Science+Business Media, LLC, part of Springer Nature 2021

Abstract

The oxidation resistance of TiAl alloy is still a problem in air above 800 °C. Gadolinium is an active element which is known to improve the oxidation resistance of Mg alloy. Very dense TiAl-Gd alloys with several compositions were prepared by spark plasma sintering (SPS). Isothermal oxidation testing of sintered alloy in air at 800 °C was carried out for 500 h. The sintering microstructure, oxidation kinetics, oxide-layer structure and oxidation mechanism were systematically studied. The results show that Gd-containing TiAl alloy shows improved oxidation resistance at high temperature compared with alloy without Gd. The Gd-rich phase distributed along the boundary of powder particles can hinder the outward diffusion of Ti and Al and preferentially consume oxygen in the matrix, thus inhibiting the growth of oxide scale and improving the spalling resistance of TiAl alloy. TiAl-0.3Gd alloy has excellent oxidation resistance, with the lowest mass gain and the thinnest oxide scale of 2.64 mg/cm² and 19.7 μm, respectively. This result will lay a foundation for the design of TiAl-based alloy with high-temperature oxidation resistance.

✉ Hongliang Sun
sunhld@163.com

Qianqian Guo
swjtugqq@163.com

Zhengkun Cai
caizkd@163.com

Yuxing Deng
huangliansqw@163.com

Xiaosong Jiang
xsjiang@home.swjtu.edu.cn

Song Chen
schen2012@home.swjtu.edu.cn

¹ School of Materials Science and Engineering, Southwest Jiaotong University, Chengdu 610031, Sichuan, China

Keywords TiAl alloys · High-temperature oxidation · Gd addition · SPS

Introduction

TiAl alloys have excellent physical and mechanical properties such as low density, high specific strength and excellent creep resistance and have become a potential high-temperature structural material to replace nickel-based superalloy in aerospace engineering in recent years [1, 2]. It has been used in the structure of new generation turbine engine at 550–750 °C [2–4]. However, due to its poor ductility and machinability at room temperature, the development of TiAl alloys is still a great challenge. To solve this problem, a lot of research has been done in the preparation process of TiAl alloy. The general method is to add alloying elements, such as Mn, V, Cr, Mo and Zr [5, 6], which can reduce the grain size of TiAl-based alloy, thus leading to the improvement of ductility, but these elements will reduce the oxidation resistance of the alloy.

Therefore, spraying coating on the surface of TiAl alloys or adding other elements to TiAl alloy has been used to improve the high-temperature oxidation resistance of TiAl alloy [7–9]. Due to doping effect, W and Nb reduce the ability to form interstitial oxygen and Ti vacancy, thus restraining the formation of titanium oxide, and encouraging the formation of alumina by improving the activity of Al. Compared with the TiO₂ layer, the Al₂O₃ layer is a denser, more adhesive and protective oxide scale, so W and Nb improve the oxidation resistance of the alloy [10–13]. Ta can equally displace Nb, because they belong to the same group on the periodic table of the elements, which indicates that the chemical behaviors of these two elements are similar [6]. In addition, Ta has a higher melting temperature, which makes it possible to increase the service temperature of TiAl alloys [6]. Besides, Sn and Co elements will form a Sn/Co-rich layer at the interface between the oxide scale and substrate, which hinders the inward diffusion of O and the outward diffusion of Ti and Al, thus preventing the growth of the oxide scale [12, 14]. Similarly, rare earth element Y has been proved to form YAl₂ phase at the grain boundary [11, 15, 16], which advances the selective oxidation of Al, inhibits the growth of TiO₂ layer and improves the adhesion of the oxide scale. However, excessive Y will cause internal oxidation, which will detrimentally influence the oxidation resistance of the alloy [11, 17].

Gd is also a rare earth element, which can reduce interlayer spacing and particle size, thereby improving the plasticity and strength of TiAl alloy and reducing the creep rate of TiAl alloy [18–21]. Meanwhile, adding Gd to Mg alloys will change the type and distribution of the second phase and advance the oxidation resistance of Mg alloy [22]. Nevertheless, little research has been done on its oxidation resistance, so it is important meaning to study the comprehensive effect of Gd on the oxidation resistance of TiAl alloy. In order to study the effect of Gd on the oxidation behavior of Ti-48Al-2Cr-2Nb alloy at high temperature, TiAl alloys with different compositions were sintered by spark plasma sintering (SPS), and isothermal oxidation tests were carried out in air. The microstructure, oxidation kinetics, oxide layer structure

and oxidation mechanism of the sintered samples were comprehensively studied. This work will likely facilitate the development of powder metallurgy for TiAl alloy.

Material and Methods

The alloys with chemical compositions of Ti-48Al-2Cr-2Nb-xGd ($x=0, 0.15, 0.3$, at.%) (here after known as TiAl-0Gd, TiAl-0.15Gd and TiAl-0.3Gd alloy, severally) were prepared using powder metallurgy. Gas-atomized pre-alloyed (PA) Ti-48Al-2Cr-2Nb powder (particle size of 100 mesh) was mixed with pure Gd powder (particle size of 300 mesh) in a planetary ball mill for 4 h at 300 rpm and then vacuum freeze-dried for 24 h. The samples were fabricated in a LABOX-650F spark plasma sintering furnace at argon protective atmosphere for sintering. The samples were kept at 1200 °C sintering temperature and 40 MPa sintering pressure for 5 min, and the heating rate was 100 °C. When the temperature was below 50 °C, the sample was taken out of the furnace, then the graphite paper on the sample surface was removed, and the sample density was surveyed by Archimedes Drainage Method.

The specimens for isothermal oxidation tests were rectangular parallelepiped prepared by Wire cut Electrical Discharge Machining with sizes of $4 \times 4 \times 8$ mm³. Before isothermal oxidation test, the six surfaces of each sample were milled with 600 mesh sandpapers and ultrasonically cleaned with ethanol for 15 min. Isothermal oxidation tests were carried out at 800 °C in a chamber-type electric resistance furnace in static air. The samples were placed in corundum crucible baked to constant weight and put into the furnace for oxidation. The samples were taken out from the furnace every once in a while then 20 min of cooling in air, and their weight was measured using an analytical balance with an accuracy of 0.1 mg. Three specimens were tested under uniform circumstances to guarantee the accuracy of the data. The preparation process of samples and the oxidation test are shown in Fig. 1.

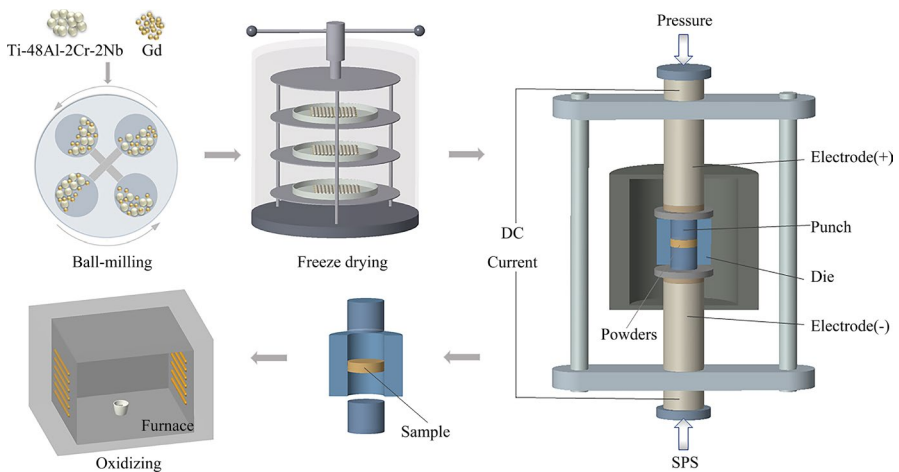


Fig. 1 Diagrammatic sketch of the experimental route used in the work

The density of sintered samples was measured using Archimedes drainage method. For the purpose of investigating the microstructure of the sintered sample and the oxidized cross-sectional, both samples before and after oxidation were steadily milled to 2000 mesh using SiC sandpapers and immediately polished with 2.5 μm diamond particles, and finally ultrasonically cleaned with ethanol and dried. The initial microstructure of the sintered samples and the cross-sectional morphology of the oxidized samples were detected by the backscattered electron (BSE) mode of field emission scanning electron microscopy (SEM, JSM-7800F) equipped with energy-dispersive spectroscope (EDS, OXFORD X-Max 80), and the surface morphology of the oxidized samples was observed by the secondary electron (SE) mode. The phase constitution of the sintered samples and oxidation products was measured by an X-ray diffractometer (XRD, EMPYREAN) with Cu $K\alpha$ radiation.

Results

Material Characterization

Figure 2 demonstrates the microstructure of the sintered TiAl-xGd ($x=0, 0.15, 0.3$) alloys. It can be clearly observed that all three alloys display a sufficiently dense microstructure (99.3% of theoretical density), which also shows that SPS can obtain completely compact structure at relatively low temperature (Fig. 2a–f). The microstructure in the Gd-free sample is characterized by the majority of γ grains and a few of α_2 -Ti₃Al + γ -TiAl lamellae [23–25]. Aside from grains and lamellae, bright white phases are distributed at the boundaries of powder particles in the microstructure of alloy containing Gd. In order to further study the composition of the additional phase, EDS mapping was made for the additional phase (Fig. 2g). According to the figure, the white phase has two different compositions, one of which is oxygen-rich phase and is presumed to be Gd₂O₃, and the other is oxygen-free and should be metal Gd (yellow ellipse in Fig. 2g). XRD results (Fig. 3) also confirmed that the main phase of the three alloys was γ phase, and a small amount of α_2 phase was found. Meanwhile, Gd₂O₃ peak was found in the alloy containing Gd. This is consistent with the morphological photos and EDS results. However, due to the small amount of Gd, no other Gd-containing phases were found in the XRD spectrums, which may require a more precise analysis method.

Isothermal Oxidation Kinetics

The oxidation kinetics curves of TiAl-xGd ($x=0, 0.15, 0.3$) alloys after isothermal oxidation at 800°C are illustrated in Fig. 4. As shown in the figure, the mass of all alloys increases following the rise of oxidation time, which is identified with some previous studies on GE48 alloy. At the same time, it can be discovered from the figure that the weight gain of these alloys declines with the addition of Gd. For instance, the TiAl-0.3Gd alloy has a weight gain of 2.64 mg/cm², much less

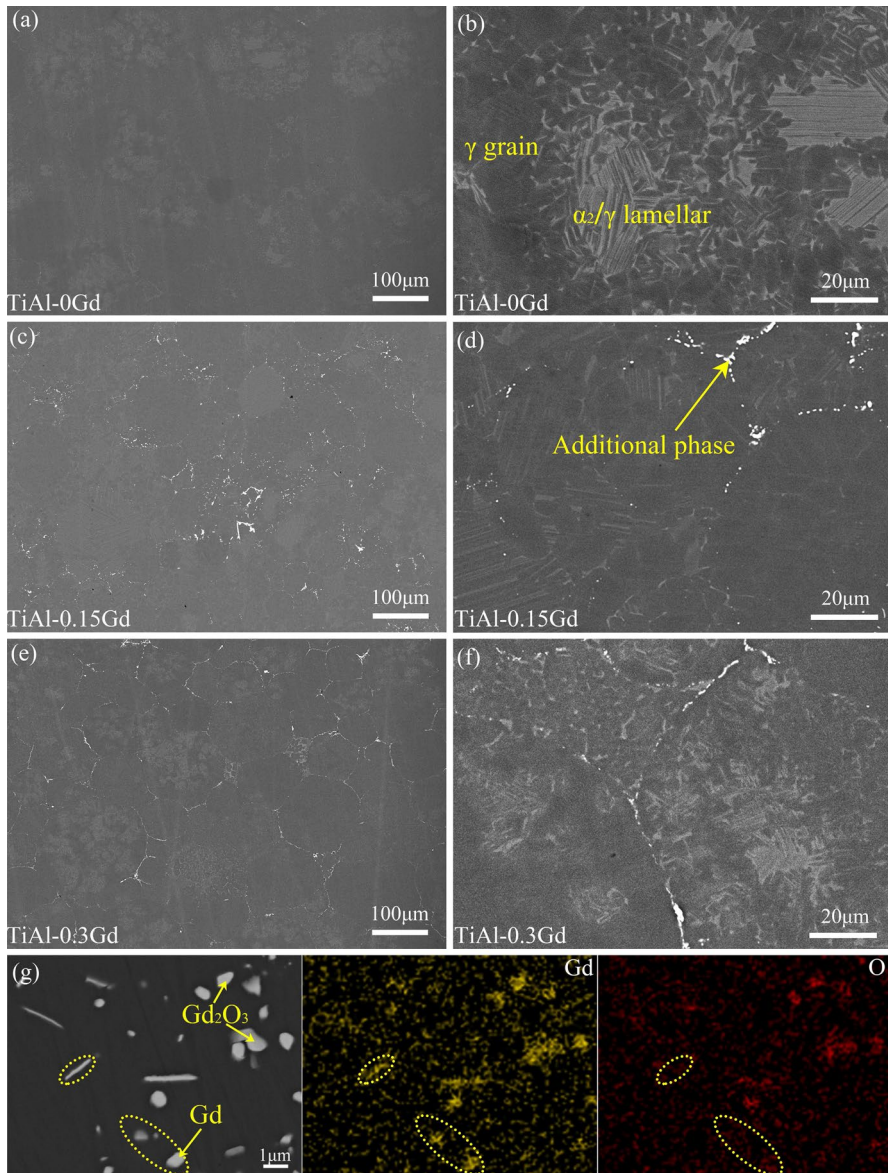


Fig. 2 BSE micrographs of the microstructure of **a, b** TiAl-0Gd; **c, d** TiAl-0.15Gd; **e, f** TiAl-0.3Gd alloys and **g** morphology and EDS mapping of TiAl-0.3Gd alloy

than that of TiAl-0Gd alloy (3.36 mg/cm^2) after 500 h of oxidation. The relation of weight change with oxidation time can be fitted using the subsequent formula [12]:

$$\Delta M^n = k_n t \quad (1)$$

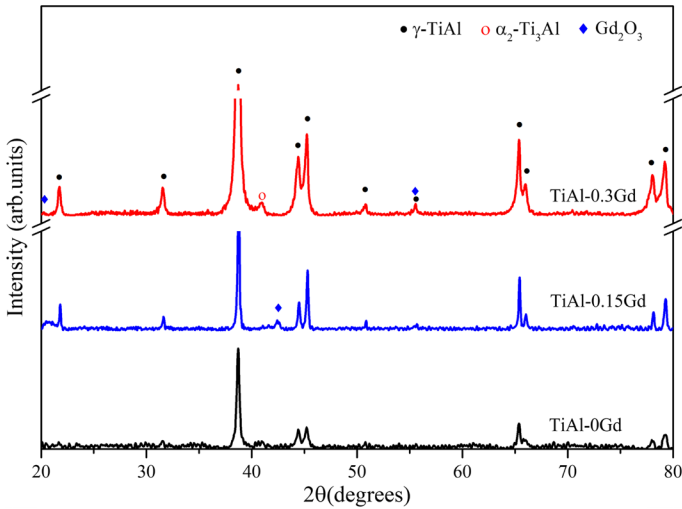


Fig. 3 XRD patterns of TiAl-xGd ($x=0, 0.15, 0.3$) alloys

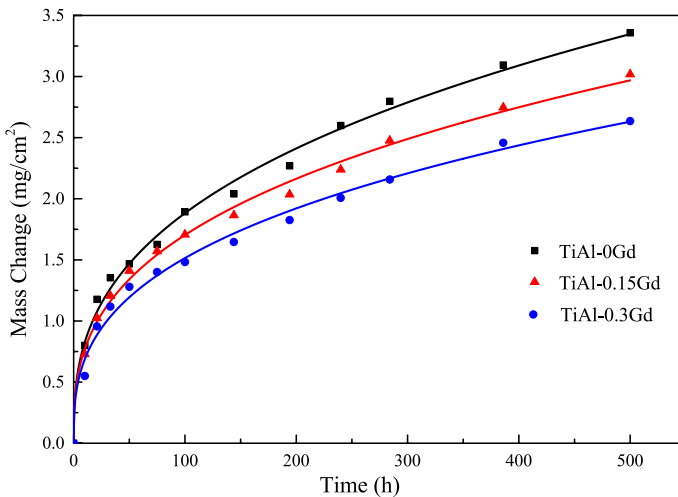


Fig. 4 Oxidation kinetics of TiAl-xGd ($x=0, 0.15, 0.3$) alloys at 800 °C

In the formula, ΔM denotes the weight change per unit area (mg/cm^2), n means the oxidation exponent, k_n is the oxidation reaction rate constant ($\text{mg}^n\text{cm}^{-2n}\text{h}^{-1}$), and t is the oxidation time (h). Origin software was used to fit the experimental data on the basis of Eq. (1) until the theoretical curve is close to the experimental curve, and the corresponding value of n and k_n was gained. The gained fitting curves and calculated parameters are shown in Fig. 4 and Table 1, respectively. The fitting results indicate that the n values of 0Gd, 0.15Gd and 0.3Gd alloys are 2.7952, 2.8972 and 2.9293, respectively. It is worth noting that there is a certain relationship

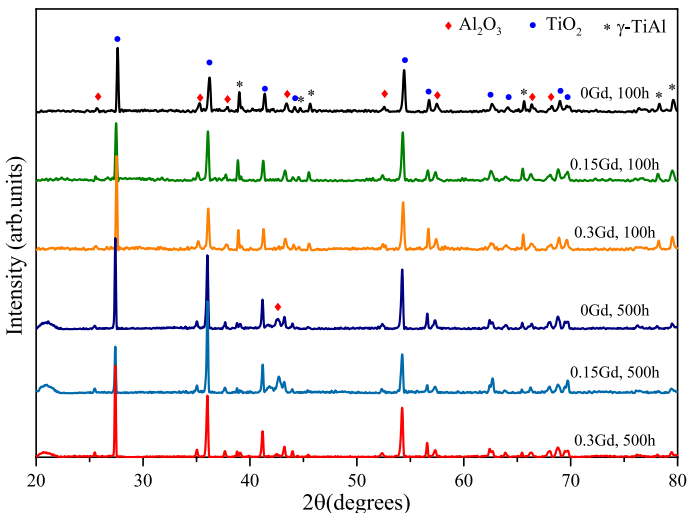
Table 1 Calculated values of n and oxidation rate constants (k_n , $\text{mg}^n\text{cm}^{-2n}\text{h}^{-1}$) for the oxidized specimens at 800 °C

	TiAl-0Gd	TiAl-0.15Gd	TiAl-0.3Gd
n	2.7952	2.8972	2.9293
k_n	0.0586	0.0468	0.0337

between the value of n and oxidation kinetics; that is, $n = 1, 2$ and 3 are equivalent to linear kinetics, parabolic kinetics and cubic kinetics, respectively [26]. Therefore, the oxidation behavior of the studied alloys approximately abides by the cubic kinetic model. The oxidation resistance of the alloy increases with the increase of oxidation exponent n , and decreases with the increase of oxidation rate constant k_n . Therefore, the addition of Gd can ameliorate the oxidation resistance of TiAl alloy in effect, and the alloy with 0.3Gd has the best oxidation resistance. L. Mengis et al. [27] studied the oxidation resistance of GE 4822 alloy between 600 and 900 °C, and the results showed that at 800 °C, the weight gain after 100 h isothermal oxidation was 1.54 mg/cm^2 . In this experiment, the TiAl-0Gd alloy has a weight gain of 1.89 mg/cm^2 at 100 h, and even TiAl-0.3Gd has a weight gain of 1.48 mg/cm^2 . This may be because the oxygen content in PM TiAl is usually higher than that in casting and forging TiAl [28].

Surface Morphology After Isothermal Oxidation

XRD was used to check the oxidized surfaces of the three alloys to research the phase composition of oxide scale, and the results are displayed in Fig. 5. The oxidized surfaces of the three alloys are principally composed of TiO_2 and Al_2O_3 , which is basically because of their parallel growth kinetics. Due to the small

**Fig. 5** XRD spectra of TiAl-xGd ($x = 0, 0.15, 0.3$) alloys after isothermal oxidation for different time

thickness of the oxide scale, peaks of γ -TiAl were observed in the oxidized samples for 100 h, while γ -TiAl peak intensity was decreased in the oxidized samples for 500 h, indicating that the oxide scale thickness increases with increasing time. Generally speaking, the major phase composition of the oxide scale is not changed after adding Gd, because the constituents of the oxide surfaces in these three alloys are extremely similar.

The surface morphology of the three alloys after isothermal oxidation at 800 °C for 10 h is illustrated in Fig. 6. Spherical and acicular oxides are distributed on the oxidation surfaces of the three alloys, and EDS shows that the oxidation products of these two shapes are the mixture of TiO_2 and Al_2O_3 . The reason for the formation

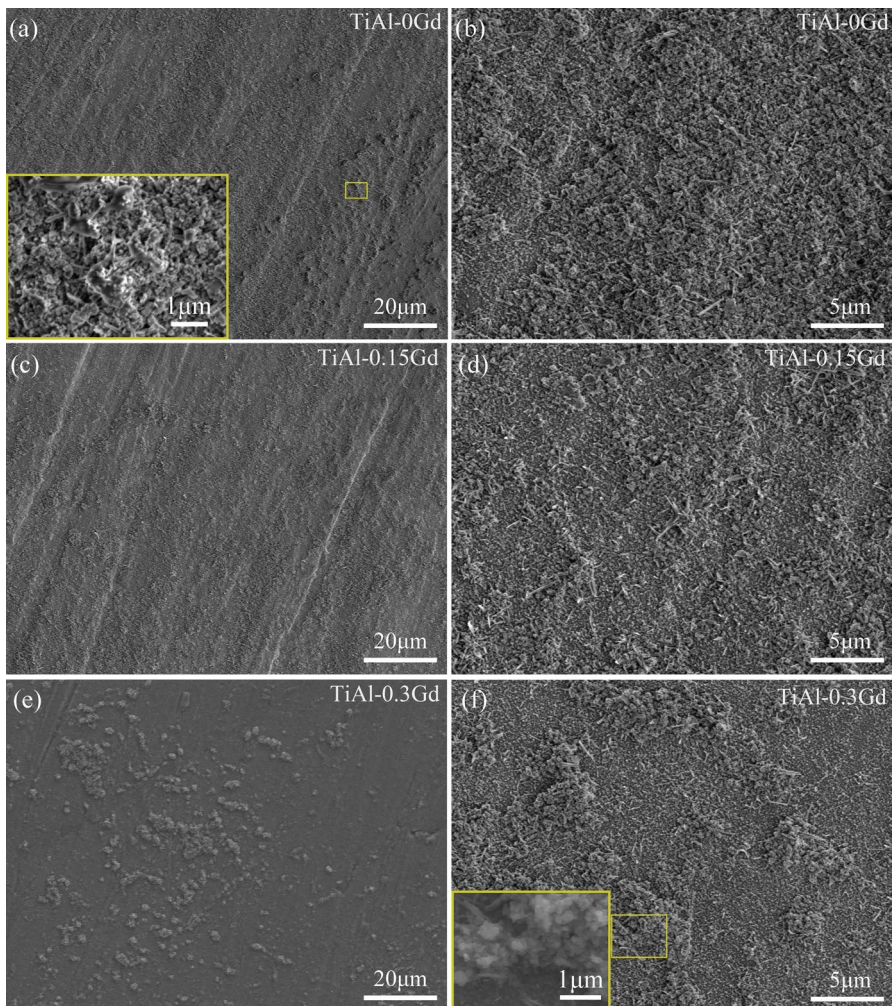


Fig. 6 Surface morphologies of the alloys after isothermal oxidation at 800 °C for 10 h. **a, b** TiAl-0Gd; **c, d** TiAl-0.15Gd; **e, f** TiAl-0.3Gd

of this mixed oxide is due to the similar thermodynamic stability of Al_2O_3 and TiO_2 at high temperature. In addition, it can be observed from the enlarged picture in the yellow box in Fig. 6a that the black part of the oxidized surface is formed by the coarsening and adhesion of oxides, but this situation is not found in the alloy containing Gd.

Figure 7 is the surface morphology of three alloys oxidized for 100 h and 500 h. Compared with the surface oxidized for 10 h, the surface oxidized for 100 h is more serious, and the morphology of oxide changes from spherical to coarse irregular columnar crystal. These irregular columnar crystals are confirmed to be TiO_2 by EDS, which means that with the increase in time, the outermost layer of oxide scale is no longer a mixture of TiO_2 and Al_2O_3 , but is basically covered by TiO_2 . By contrasting the morphology for 100 h, it can be perceived that the titanium dioxide particles on the surface are arranged more closely and the particle size is uniform after adding Gd. The oxide sizes on the surface of Gd-free alloy in Fig. 7a are different, and there are many gaps between grains. In addition, with the time extended to 500 h, the titanium dioxide particles on the oxidized surface grew 2~3 times. When oxidized for 500 h, there is no obvious difference between the surfaces of several alloys, which may be because titanium dioxide grows and connects with each other with the increase of time, and there is no more space for lateral growth.

Cross-Sectional Observations of Oxide Scale

The cross-sectional microstructures of the oxide scale for TiAl-xGd ($x=0, 0.15, 0.3$) alloys after isothermal oxidation for 100 h are shown in Fig. 8. It can be clearly seen that for TiAl-0Gd and TiAl-0.15Gd alloys, some voids are observed in the oxide layer. On the contrary, there are basically no voids in the oxide layer of the alloy with more Gd content, showing a uniform and completely adhered oxide scale. The average thickness of the oxide scale of TiAl-0Gd

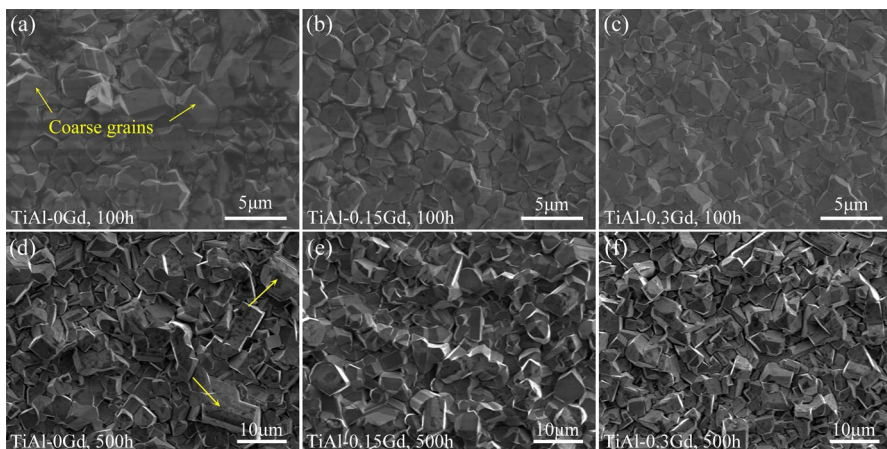


Fig. 7 Surface morphologies of the alloys after isothermal oxidation at 800 °C for 100 h: **a** TiAl-0Gd , **b** TiAl-0.15Gd , **c** TiAl-0.3Gd and for 500 h: **d** TiAl-0Gd , **e** TiAl-0.15Gd , **f** TiAl-0.3Gd

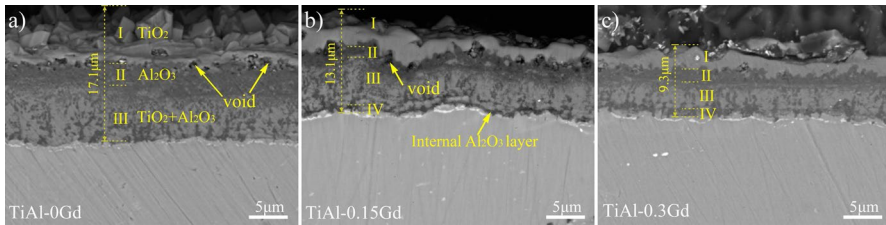


Fig. 8 BSE micrographs of the cross-sectional morphologies on **a** TiAl-0Gd, **b** TiAl-0.15Gd, **c** TiAl-0.3Gd alloys after isothermal oxidation at 800 °C for 100 h

alloy is 17.1 μm , TiAl-0.15Gd alloy is 13.1 μm , and TiAl-0.3Gd alloy is 9.3 μm (Fig. 8a–c). Therefore, the TiAl-0.3Gd alloy shows the slowest oxidation rate, while the alloy without Gd has the fastest oxidation rate, which is consistent with the weight gain results (Fig. 4).

Figure 9 exhibits the cross-sectional EDS mapping of the alloy after oxidation at 800 °C for 100 h. It can be seen from the comparison that the alloy without Gd is composed of three layers. The external scale (I) of the alloy is mainly composed of loose and porous TiO_2 rutile (relatively bright phase, rich in Ti and O as determined by EDS mapping). The sub-layer (II) of oxide scale is dominated by discrete Al_2O_3 oxides (dark phase), followed by an inner layer (III) of the mixed TiO_2 and Al_2O_3 . However, by observing the morphology in Fig. 8 and the surface scanning in Fig. 9, it can be found that a thin dark gray oxide layer should be Al_2O_3 layer (IV) at the interface between oxide scale and matrix in Gd-containing alloy. At the same time, although the Al_2O_3 layer in oxide scale of TiAl-0.3Gd alloy is thinner than that of Gd-free alloy, the thickness of TiO_2 layer and mixed layer is also reduced by about half, and the alumina layer in the alloy containing Gd is continuous and dense, which has good protection. This shows that the addition of Gd can significantly improve the oxidation resistance of TiAl alloy at high temperature. Moreover, the enrichment of Nb and N was found at the interface between scale and substrate in all alloys. The research shows that a certain amount of TiN layer formed at the interface will reduce the activity of titanium and increase the activity of aluminum [27]. However, when TiN content is too high, the nitride will be oxidized to form titanium oxide, which will adversely affect the oxidation resistance of the alloy [12].

Over time, the thickness of the scale of the three alloys increased (Fig. 10), but up to 500 h, the scale did not peel off. At this time, the average thickness of the oxide scale of TiAl-0Gd, TiAl-0.15Gd and TiAl-0.3Gd alloy is 29.3 μm , 25.9 μm and 19.7 μm , respectively. Combined with the surface scanning results in Fig. 11, it can be seen that the scale structure of the three alloys has no obvious change compared with that at 100 h, but for TiAl-0Gd alloy, transverse cracks exist at the interface between oxide layer and substrate, and the TiO_2 and Al_2O_3 mixed layer is easy to peel off when cooling. It can be speculated that these scales will peel off soon, which will adversely affect the oxidation resistance of the alloy. As for Gd-containing alloys, the oxide scale keeps a satisfactory combination with the

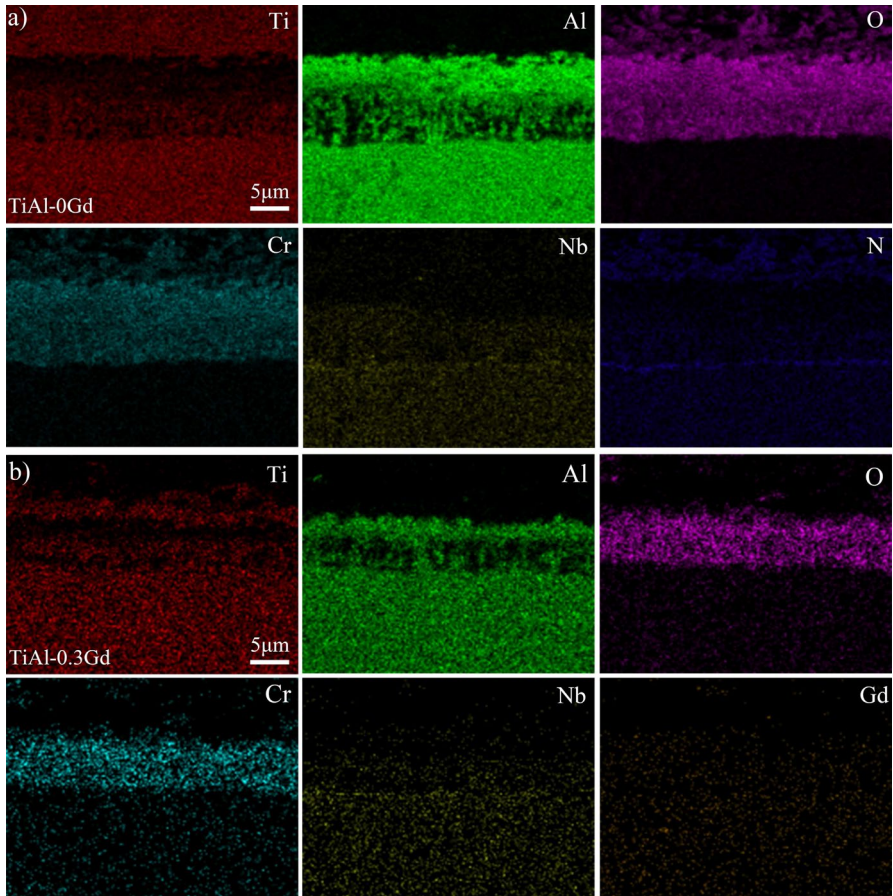


Fig. 9 The EDS mapping of the alloy cross section after oxidation at 800 °C for 100 h. **a** TiAl-0Gd; **b** TiAl-0.3Gd

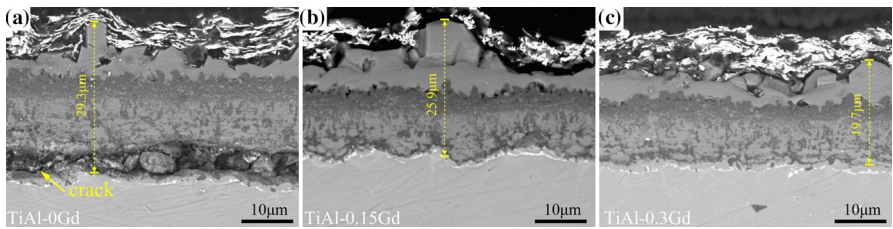


Fig. 10 BSE micrographs of the cross-sectional morphologies on **a** TiAl-0Gd, **b** TiAl-0.15Gd, **c** TiAl-0.3Gd alloys after isothermal oxidation at 800 °C for 500 h

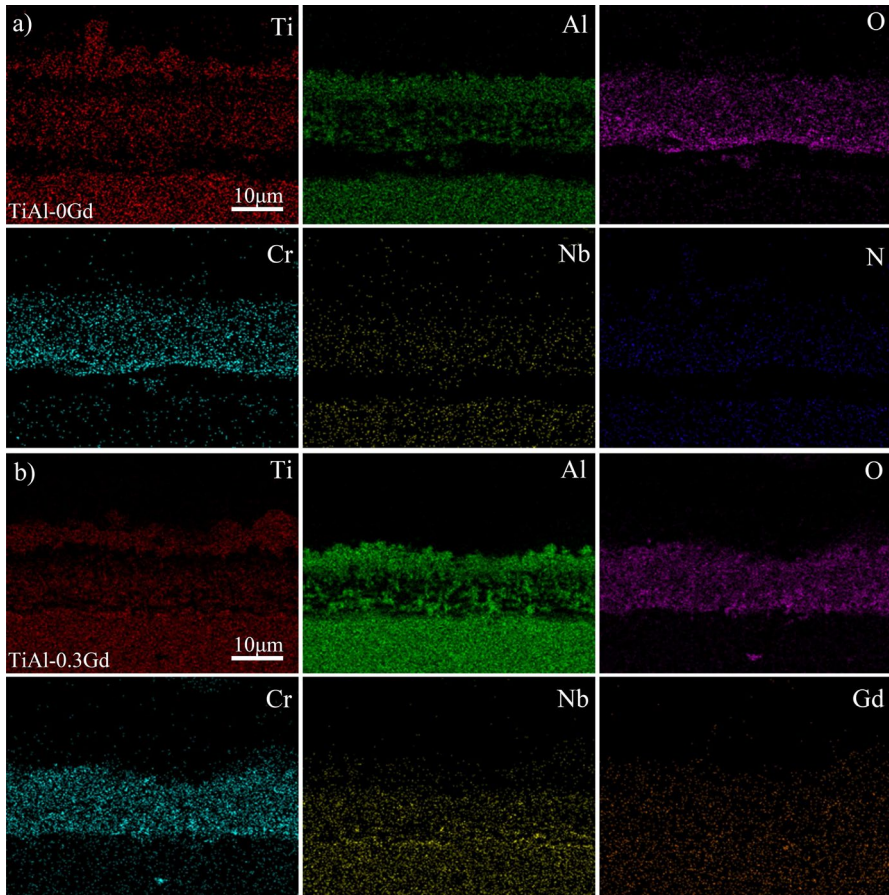


Fig. 11 The EDS mapping of the alloy cross section after oxidation at 800 °C for 500 h. **a** TiAl-0Gd; **b** TiAl-0.3Gd

substrate and no any crack could be observed, which indicates the Gd addition offers a better oxide scale adhesion.

Discussion

According to the above consequences, the oxidation mechanism of TiAl-0Gd and TiAl-0.3Gd alloys after isothermal oxidation at 800 °C for 500 h is diagrammatically summarized in Fig. 12. For TiAl-0Gd alloy, because Cr and Nb are uniformly dissolved in the matrix, the matrix is composed of γ -TiAl and α_2 -Ti₃Al phases. In the process of high-temperature oxidation, the oxidation dynamics of Ti and Al elements can be reckoned by means of Gibbs free energy, as noted below [29]:

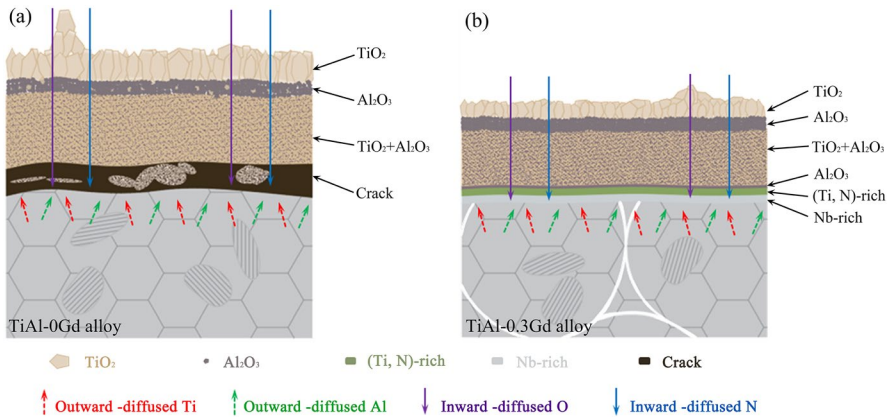


Fig. 12 Diagrammatic drawing of the oxidation mechanism for **a** TiAl-0Gd and **b** TiAl-0.3Gd alloys after isothermal oxidation at 800 °C for 500 h

$$\Delta G_{TiO_2} = 943490 + 179.08T(298 \sim 1940K) \tag{2}$$

$$\Delta G_{Al_2O_3} = 1120480 + 214.22T(932 \sim 2345K) \tag{3}$$

In the formula, T is the temperature (K). In view of Eqs. (2) and (3), the Gibbs free energy of formation of TiO₂ at 800 °C is –751.3 kJ mol⁻¹, and that of Al₂O₃ at 800 °C is –890.6 kJ mol⁻¹. Therefore, it can be inferred that Al is more susceptible to oxidation than Ti. However, the diffusivity of Ti in γ phase is greater than that of Al in γ phase [30], and the diffusivity of O in TiO₂ is much greater than that of O in Al₂O₃ [31], the growth activation energy of TiO₂ is much lower than that of Al₂O₃, which leads to a lower growth rate of Al₂O₃ [26]. At the same time, because the diffusion rate of Ti in TiO₂ is faster than that of oxygen, while the diffusion rate of Al in Al₂O₃ is slower; this causes TiO₂ to grow outward to the gas oxide interface and Al₂O₃ grows inward at the metal-oxide interface [6]. Therefore, although a mixture of Al₂O₃ and TiO₂ is formed in the initial stage of oxidation, as the oxidation time increases, an outer layer of TiO₂ and an inner layer of Al₂O₃ are finally formed [26]. Single and continuous Al₂O₃ can be used as a protective layer, because it is dense enough to effectively block oxygen diffusion, but porous and loose TiO₂ is not conducive to oxidation resistance, which provide paths for short-circuit diffusion of oxygen and give rise to successive oxidation [14], eventually forming a multi-layer oxide scale structure. At the same time, the cross-sectional micrographs of all alloys show that the mixed layer of titanium oxide and aluminum oxide occupies the largest scale volume.

The results show that the addition of Gd will reduce the crystallite dimension and interlayer spacing of the alloy, and the diffusion process is inhibited by Gd atoms on the grain boundary [18–20, 32]. Due to the low solubility of yttrium in titanium dioxide and alumina oxides, Y₂O₃ precipitation leads to an evident grain refinement

effect and a decrease in oxygen diffusion rate, and the reaction between oxygen and Ti is inhibited [33]. Similarly, because Gd is distributed at the boundary of powder particles and has a strong affinity for oxygen, it will adsorb oxygen in the matrix, thus forming Gd_2O_3 and blocking the diffusion path. On the basis of the Van't Hoff equation, the change of Gibbs free energy during oxidation can be expressed as [11]:

$$\Delta G = RT \ln \frac{p'_{O_2}}{p_{O_2}} \quad (4)$$

where p'_{O_2} manifests the equilibrium oxygen partial pressure of oxidation reaction or decomposing pressure of oxide at the reaction temperature, and p_{O_2} means the oxygen partial pressure of the oxidation circumstances. The condition for oxidation reaction is $\Delta G < 0$, and then $p'_{O_2} < p_{O_2}$ is required. The ΔG^0 -T diagram plotting by Ellingham demonstrates that the p'_{O_2} of Al (10^{-44} atm) is smaller than of Ti (10^{-35} atm) at 800 °C [4]. Therefore, under low oxygen partial pressure, Al is preferentially oxidized. Due to the low oxygen partial pressure under the oxidized scale [11], a thin aluminum layer is formed under the oxidized scale, which further prevents the inward diffusion of oxygen and improves the oxidation resistance of the alloy. It can also be seen from the weight increase curve in Fig. 4 and the cross-sectional morphology (Figs. 8–11) that the oxidation weight gain is greatly decreased after adding Gd, and the thickness of the alloy oxide scale is reduced by about half after adding 0.3 at. % Gd at 100 h.

The results show that alloying elements have a momentous influence on the oxidation behavior of TiAl alloys. When the concentration of Cr is less than 4 at. %, it is harmful, which may be put down to doping effect [6], which will lead to the increase of O_2 vacancy concentration, and the concentration of O_2 vacancy is responsible for oxygen diffusion [34], which leads to the acceleration of the growth rate of TiO_2 . Nb is considered to be a doping element with a higher valence than Ti. By reason of the electron neutrality in the oxide, it will reduce the ability of interstitial oxygen and titanium vacancy formation, thus reducing the diffusion of oxygen and titanium correspondingly and inhibiting the growth of rutile [35]. The addition of Nb also has other effects on oxidation behavior, such as fortifying the activity of Al, reducing the solubility of O in the alloy, and advancing the formation of TiN at the interface between substrate and scale, thus preventing the diffusion of Ti and O ions [11].

In this experiment, Cr can be found to diffuse outward in the oxidation of all alloys, and it has diffused to TiO_2 layer in Gd-free alloy at 100 h. Fa et al. [36] used the first principles to study and calculate, which showed that Cr not only reduced the formation energy of oxygen vacancy in TiO_2 and promoted the growth of TiO_2 , but also improved the relative stability of Al_2O_3 to TiO_2 , which eventually led to internal oxidation. In addition, in all alloys, it is found that Ti and N are enriched at the scale/matrix interface, and there is a Nb-rich layer below it, which is very common in the oxidation of TiAl alloy containing Nb, because Nb does not diffuse outward with titanium and aluminum atoms, but remains in the matrix [10], so adding Gd has little effect on the diffusion of Nb.

During the oxidation process, the oxide/substrate composites experienced continuous thermal fatigue because samples were taken out periodically and weighed in air cooling. The mismatch between thermal expansion coefficients of TiN and oxide or substrate results in thermal stress at the interface [37]. In addition, since TiO_2 (1.73) has a larger Pilling-Bed-worth ratio (PBR), there is high compressive stress in the oxide scale during oxidation. With the rapid growth and thickening of the oxide scale, the compressive stress gradually increases. Further, the surface layer of the scale is simultaneously subjected to tensile stress [14]. Cyclic stress changes near the interface caused by repeated heating/cooling under oxidation test may accelerate the separation of complete oxides under isothermal oxidation [37]. Therefore, in view of the above effects, when the oxidation time is increased to 500 h, a wide crack can be found at the interface between oxide scale and substrate, and the oxide layer has broken here, so the oxide layer is in danger of falling off (Fig. 10a). In Gd-containing alloys, the diffusion path is blocked and the rapid growth of TiO_2 is inhibited, which makes the thickness of oxide scale much smaller than that of TiAl-0Gd alloy, relieves the internal pressure of oxide scale, and improves the adhesion and spalling resistance of oxide scale, which is found in many TiAl alloys with rare earth elements [11, 38–41].

Conclusions

In this paper, Ti-48Al-2Cr-2Nb alloys with diverse Gd additions were successfully prepared by SPS and their oxidation behaviors were investigated through air isothermal oxidation at 800 °C for 500 h. The primary conclusions are summarized as follows:

(1) A completely compact structure can be obtained by sintering at 1200 °C using SPS route. The microstructure of Gd-containing alloy consists of matrix phase γ grains + α_2/γ lamellae and Gd_2O_3 particles distributed along the boundary of powder particles.

(2) The addition of Gd can significantly improve the oxidation resistance of TiAl alloys at high temperature. After isothermal oxidation for 500 h, the TiAl-0.3Gd alloy displays the minimum mass increment of 2.64 mg/cm², thinnest oxide scale thickness of 19.7 μm and without surface flaking and flaw formation.

(3) The addition of Gd will change the structure of the alloy scale. After adding Gd, the scale structure of the alloy is loose porous TiO_2 layer/thin but continuous dense Al_2O_3 layer/mixed TiO_2 + Al_2O_3 layer/thin Al_2O_3 layer.

(4) Gd addition can heighten the anti-peeling ability of the oxide scale in TiAl alloys. The existence of the Gd-rich phases distributed along the particles boundaries and the Al_2O_3 layer above the matrix can inhibit the inward diffusion of O and the outward diffusion of Ti and Al, sequentially restraining the growth of oxide scale and alleviating the stress state in the oxide scale. It is beneficial to improve the spalling resistance and oxidation resistance of TiAl alloys at high temperature.

Acknowledgements This research was sponsored by the National Key Research and Development Program of China (No. 2016YFB1200505) and Cultivation project for original scientific research instruments and equipment of Southwest Jiaotong University (NO. XJ2021KJZK041).

References

1. H. Sun, Z. Wang, Y. Du, and J. Yuan, Densification mechanism and microstructure evolution of Ti-48Al-2Cr-8Nb alloy by spark plasma sintering. *Cryst Res Technol.* **54**, (11), 2019 (1900107).
2. H. W. Liu, D. P. Bishop, and K. P. Plucknett, Densification behaviour and microstructural evolution of Ti-48Al consolidated by spark plasma sintering. *J Mater Sci.* **52**, 2017 (613–627).
3. R. Muñoz-Moreno, E. M. Ruiz-Navas, B. Srinivasarao, and J. M. Torralba, Microstructural development and mechanical properties of PM Ti-45Al-2Nb-2Mn-0.8 vol.%TiB2 processed by field assisted hot pressing. *Journal of Materials Science and Technology.* **230**, 2014 (1145–1154).
4. M. P. Bacos, S. Ceccacci, J. P. Monchoux, et al., Oxidation behavior of a spark plasma sintered Ti-48Al-2W-0.1B alloy at 800 °C. *Oxid Met.* **93**, 2020 (587–600).
5. Y. Garip and O. Ozdemir, A study of the cycle oxidation behavior of the Cr/Mn/Mo alloyed Ti-48Al-based intermetallics prepared by ECAS. *J Alloys Compd.* **818**, 2020 (152818).
6. P. V. Cobbinah, W. Matizamhuka, R. Machaka, M. B. Shongwe, and Y. Yamabe-Mitarai, The effect of Ta additions on the oxidation resistance of SPS-produced TiAl alloys. *Int J Adv Manuf Tech.* **106**, 2020 (3203–3215).
7. N. Laska, R. Braun, and S. Knittel, Oxidation behavior of protective Ti-Al-Cr based coatings applied on the γ -TiAl alloys Ti-48-2-2 and TNM-B1. *Surf Coat Technol.* **349**, 2018 (347–356).
8. K. Zhang, L. Xin, Y. Lu, et al., Improving oxidation resistance of γ -TiAl based alloy by depositing TiAlSiN coating: effects of silicon. *Corros Sci.* **179**, 2021 (109151).
9. R. Swadźba, L. Swadźba, B. Mendala, P.-P. Bauer, N. Laska, and U. Schulz, Microstructure and cyclic oxidation resistance of Si-aluminide coatings on γ -TiAl at 850 °C. *Surf Coat Technol.* **403**, 2020 (126361).
10. P. Zhao, X. Li, H. Tang, et al., Improved high-temperature oxidation properties for Mn-containing Beta-Gamma TiAl with W addition. *Oxid Met.* **93**, 2020 (433–448).
11. L. L. Zhao, G. Y. Li, L. Q. Zhang, et al., Influence of Y addition on the long time oxidation behaviors of high Nb containing TiAl alloys at 900 °C. *Intermetallics.* **18**, 2010 (1586–1596).
12. Y. Pan, X. Lu, M. D. Hayat, et al., Effect of Sn addition on the high-temperature oxidation behavior of high Nb-containing TiAl alloys. *Corros Sci.* **166**, 2020 (108449).
13. D. Pilone, F. Felli, and A. Brotzu, High temperature oxidation behaviour of TiAl-Cr-Nb-Mo alloys. *Intermetallics.* **43**, 2013 (131–137).
14. Y. Pan, X. Lu, T. Hui, et al., High-temperature oxidation behaviour of TiAl alloys with Co addition. *J Mater Sci.* **56**, 2020 (815–827).
15. X. Gu, F. Cao, N. Liu, et al., Microstructural evolution and mechanical properties of a high yttrium containing TiAl based alloy densified by spark plasma sintering. *J Alloys Compd.* **819**, 2020 (153264).
16. X. Gu, S. Jiang, F. Cao, et al., A β -solidifying TiAl alloy reinforced with ultra-fine Y-rich precipitates. *Scr Mater* **192**, 2021 (55–60).
17. V. A. C. Haanappel, H. Clemens, and M. F. Stroosnijdera, The high temperature oxidation behaviour of high and low alloyed TiAl-based intermetallics. *Intermetallics.* **10**, 2002 (293–305).
18. P. V. Panin, A. S. Kochetkov, A. V. Zavodov, and E. A. Lukina, Effect of Gd addition on phase composition, structure, and properties of beta-solidifying TiAl-based alloy with Zr and Cr content variability. *Intermetallics.* **121**, 2020 (106781).
19. V. S. Sokolovsky, N. D. Stepanov, S. V. Zherebtsov, et al., The effect of Gd addition on the kinetics of $\alpha 2 \rightarrow \gamma$ transformation in γ -TiAl based alloys. *Intermetallics.* **120**, 2020 (106759).
20. K. Xia, X. Wu, and D. Song, Effects of Gd addition, lamellar spacing and loading direction on creep behaviour of a fully lamellar Ti-44Al-1Mn-2.5Nb alloy. *Acta Mater.* **52**, 2004 (841–849).
21. R. Ding, I. P. Jones, Y. Chiu, and R. Chen, Microstructure and mechanical property of directionally solidified Ti-46Al-0.5W-0.5Si alloys with and without Gd. *Intermetallics.* **20**, 2012 (123–134).

22. C. Cheng, Q. Lan, Q. Liao, et al., mEffect of Ca and Gd combined addition on ignition temperature and oxidation resistance of AZ80. *Corros Sci.* **160**, 2019 (108176).
23. Z. Trzaska, G. Bonnefont, G. Fantozzi, and J. P. Monchoux, Comparison of densification kinetics of a TiAl powder by spark plasma sintering and hot pressing. *Acta Mater.* **135**, 2017 (1–13).
24. C. Shi, K. Zhang, Z. Lu, and H. Xiao, Microstructure evolution and mechanical properties of Ti46.5Al2Cr1.8Nb-(W, B) alloys fabricated by spark plasma sintering and pulse current assisted isothermal forging. *Mater Sci Eng. A.* **747**, 2019 (98–110).
25. A. Couret, T. Voisin, M. Thomas, and J.-P. Monchoux, Development of a TiAl Alloy by Spark Plasma Sintering. *JOM.* **69**, 2017 (2576–2582).
26. Y. Garip, Investigation of isothermal oxidation performance of TiAl alloys sintered by different processing methods. *Intermetallics.* **127**, 2020 (106985).
27. L. Mengis, A. S. Ulrich, P. Watermeyer, C. H. Liebscher, and M. C. Galetz, Oxidation behaviour and related microstructural changes of two β 0-phase containing TiAl alloys between 600 °C and 900 °C. *Corros Sci.* **178**, 2021 (109085).
28. D. Zhang, N. Liu, Y. Chen, et al., Microstructure Evolution and Mechanical Properties of PM-Ti43Al9V0.3Y. *Alloy Materials.* **13**, (1), 2020 (198).
29. S. Tian, H. Jiang, G. Zhang, Y. Zhang, H. Lin, and Y. Yang, Investigation on the initial oxidation behavior of TiAl. *Alloy Mater Res Express.* **6**, (10), 2019 (106595).
30. Y. Mlshin and C. Herzig, Diffusion in the Ti-Al system. *Acta Mater.* **48**, 2000 (589–623).
31. N. S. Neelam, S. Banumathi, A. Bhattacharjee, N. R. Zafir, and M. D. Alam, Comparison of the isothermal and cyclic oxidation behavior of Cr and Mo containing γ -TiAlNb alloys. *Corros Sci.* **163**, 2020 (108300).
32. X. Wang, R. Luo, F. Liu, et al., Characterization of Gd-rich precipitates in a fully lamellar TiAl alloy. *Scr Mater.* **137**, 2017 (50–54).
33. Y. Wu, Y. Umakoshi, X. W. Li, and T. Narita, Isothermal oxidation behavior of Ti-50Al alloy with Y additions at 800 and 900°C. *Oxid Met.* **66**, 2006 (321–348).
34. Y. Garip and O. Ozdemir, Comparative study of the oxidation and hot corrosion behaviors of TiAl-Cr intermetallic alloy produced by electric current activated sintering. *J Alloys Compd.* **780**, 2019 (364–377).
35. R. Swadzba, K. Marugi, and Ł Pyclik, STEM investigations of γ -TiAl produced by additive manufacturing after isothermal oxidation. *Corros Sci.* **169**, 2020 (108617).
36. F. P. Ping, Q. M. Hu, A. V. Bakulin, S. E. Kulkova, and R. Yang, Alloying effects on properties of Al₂O₃ and TiO₂ in connection with oxidation resistance of TiAl. *Intermetallics.* **68**, 2016 (57–62).
37. D. J. Kim, D. Y. Seo, J. K. Hong, S. E. Kim, and D. Y. Keum, Cyclic-oxidation behaviours of the powder-metallurgy TiAl-4Nb-3Mn and TiAl-2Nb-2Mo beta-gamma alloys. *Can Metall Q.* **56**, 2016 (123–136).
38. Y. Tan, H. Fang, R. Chen, et al., Microalloying effects of Ho on microstructure evolution and high temperature properties of Ti46Al4Nb1Mo alloy. *Intermetallics.* **126**, 2020 (106883).
39. Zhang GY, Liu CM, Fang GL (2017) First principles studies of the influences mechanism of Y, Hf elements on the high temperature oxidation of γ -TiAl alloys. In: IOP Conference Series: Materials Science and Engineering. 167(1):012049
40. Y. Wu, S. K. Hwang, K. Hagihara, and Y. Umakoshi, Isothermal oxidation behavior of two-phase TiAl-Mn-Mo-C-Y alloys fabricated by different processes. *Intermetallics* **14**, 2006 (9–23).
41. X. Gong, R. R. Chen, H. Z. Fang, et al., Synergistic effect of B and Y on the isothermal oxidation behavior of TiAl-Nb-Cr-V alloy. *Corros Sci.* **131**, 2018 (376–385).